Available online at www.sciencedirect.com
SCIENCE DIRECT®
Journal of Nuclear Materials 327 (2004) 77–87
journal of nuclear materials
www.elsevier.com/locate/jnucmat

Fission gas release and swelling in uranium–plutonium mixed nitride fuels

Kosuke Tanaka [a,*], Koji Maeda [a], Kozo Katsuyama [a], Masaki Inoue [a], Takashi Iwai [b], Yasuo Arai [b]

[a] *Oarai Engineering Center, Japan Nuclear Cycle Development Institute, 4002 Narita-cho, Oarai-machi, Higashi-ibaraki-gun, Ibaraki-ken 311-1393, Japan*

[b] *Oarai Research Establishment, Japan Atomic Energy Research Institute, 3607 Narita-cho, Oarai-machi, Higashi-ibaraki-gun, Ibaraki-ken 311-1394, Japan*

Received 6 August 2003; accepted 6 January 2004

Abstract

Two uranium–plutonium mixed nitride, (U,Pu)N, fuel pins with different He-gap width were irradiated at a linear heating rate 75 kW/m to 4.3% FIMA in the experimental fast reactor JOYO, and nondestructive and destructive post irradiation examinations were carried out. Fission gas release rates were about 3.3% and 5.2%, and swelling rates were about 1.8% and 1.6%/% FIMA. From the radial distributions of Xe concentration measured by EPMA, it was determined that approximately 80% and 15% of fission gases were retained in the intragranular region and in the fission gas bubbles, respectively. Deformation of the fuel cladding differed between the two tested fuel pins. A uniform diameter increase was observed in the small gap fuel pin, while ovalities, which seemed to be caused by relocation of the fuel fragments, were found in the large gap one.

PACS: 28.41.Bm

1. Introduction

The Japanese Fast Breeder Reactor (FBR) program is now being directed toward establishing a reliable and economic power generation system, considering various capabilities including alternative fuel cycles. Mixed oxide (MOX) fuel has been chosen as the FBR fuel because of its chemical stability and its well-studied behavior. But MOX fuel has several inherent limitations, which include a relatively low fissile density that reduces the breeding ratio and poor thermal conductivity that restricts the linear heating rate.

Uranium–plutonium mixed nitride, (U,Pu)N, has the potential to solve these problems, because it has many favorable fuel properties, such as a high fissile density, a high melting point similar to that of MOX fuel and high thermal conductivity similar to that of metal fuel [1,2]. Advantageous thermal properties enable use of (U,Pu)N fuel at a high linear heating rate, or to application of the 'Cold Fuel Concept' [3,4] in the case of a milder linear heating rate.

The number of studies on the irradiation performance of (U,Pu)N fuel is much smaller than that of MOX fuel; studies focusing on fission gas behavior have been especially limited. Some reports have suggested that the fission gas behavior in (U,Pu)N fuel is similar to

* Corresponding author. Address: Fuel Monitoring Section, Fuels and Materials Division, Irradiation Center, Oarai Engineering Center, Japan Nuclear Cycle Development Institute, 4002 Narita-cho, Oarai-machi, Higashi-ibaraki-gun, Ibaraki-ken 311-1393, Japan. Tel.: +81-29 267 4141x5547; fax: +81-29 267 7130.

E-mail address: k-tanaka@oec.jnc.go.jp (K. Tanaka).

0022-3115/$ - see front matter © 2004 Elsevier B.V. All rights reserved.
doi:10.1016/j.jnucmat.2004.01.002

that in metal fuel rather than oxide fuel, but more studies are needed to elucidate the details.

In this study, two (U,Pu)N fuel pins were irradiated at a linear heating rate 75 kW/m to 4.3% FIMA (fraction of initial metal atom) in the experimental fast reactor JOYO. Then, nondestructive and destructive post irradiation examinations, such as profilometry, pin-puncturing test, density measurement, pore distribution measurement and electron probe microanalysis (EPMA) were carried out in hot cells. These results were compared with those in previous reports.

2. Fuel specimens and irradiation history

2.1. Fuel pin characteristics

In order to clarify the effect of gap width on the irradiation behavior, two (U,Pu)N fuel pins, L413 and L414, of different gap width were irradiated in JOYO. Table 1 shows their basic characteristics.

Fig. 1 shows a flow sheet of the fabrication process of (U,Pu)N fuel pellets and it is similar to the process reported previously [5]. Powders of PuO_2, UO_2 and graphite were weighed so as to adjust the weight ratio of $Pu/(U+Pu)$ at 0.1926 and the molar ratio of $C/(UO_2+PuO_2)$ at 2.5. These powders were mixed in a V-type blender and subsequently a ball mill, and then compacted into disks of 2–3 mm in thickness. The carbothermic reduction was carried out at 1823 K for 12 h under the flowing gas atmosphere of 92% N_2 and 8% H_2 in a furnace with a tungsten plate heater. The atmosphere in the furnace was changed with Ar gas below 1673 K during the heating-up and cooling-down stages in order to avoid the formation of higher nitrides in the fuel matrix. After heating, the formation of (U,Pu)N was identified by weight change and X-ray diffraction pattern.

The (U,Pu)N disks thus prepared were crushed in a mortar grinder and subsequently in a ball mill to obtain the sinterable powder. Two kinds of pellets having different diameters, 7.28 and 7.43 mm, were fabricated from the (U,Pu)N powder by the following method. First, the powder was mixed with pore former and then pressed into green pellets under a pressure of 2.5 ton/cm^2. The green pellets were sintered at 2003 K for 5 h under the flowing gas atmosphere of 92% Ar and 8% H_2.

After the sintering stage, the pellets were ground in a centerless grinder to satisfy the predetermined diameters. Finally, heat treatment was performed at 1773 K for 20 h under the flowing gas atmosphere of 92% N_2 and 8% H_2 to control the $N/(U+Pu)$ ratio.

When relatively large pores were introduced into the fuel matrix by sintering the pellet at high temperature with the pore former, the (U,Pu)N pellet was called a 'thermally stable pellet'. Density of the thermally stable pellet was controlled to around 85% TD (theoretical density), which aimed to mitigate the fuel cladding mechanical interaction (FCMI).

Table 2 shows the results of chemical analyses of fuel pellets. The content of tungsten (W) was higher in the L413 pellets than in the L414 pellets. In the L413 pellets, some cracks were observed after the first sintering. Therefore, these pellets were crushed again and the subsequent steps were repeated as shown in Fig. 1. The high content of W in L413 fuel pellets seemed to be introduced by this repeated process.

The (U,Pu)N fuel pellets were inserted into a cladding tube made of austenitic stainless steel, together with thermal insulator pellets of UN and reflector components. The inner and outer diameters, and thickness of the cladding tube were 7.6, 8.5 and

Table 1
Nitride fuel characteristics

Fuel pin number		L413	L414
Clading tube	Material	15Cr-20Ni stainless steel	
	Outer diameter (mm)	8.50	
	Inner diameter (mm)	7.60	
	Thickness (mm)	0.45	
Diametral gap width (mm)		0.32	0.17
Smear density (%TD)		77.8	82.2
Fuel pellet	N/M	1.00	1.01
	Diameter (mm)	7.28	7.43
	Height (mm)	~8	
	Pu/(U + Pu) (wt%)	18.6	
	U235-enrichment (wt%)	19.39	
	Bulk density (%T.D.)	84.8	86.0
	Fuel stack length (mm)	200.1	198.8

TD: theoretical density.

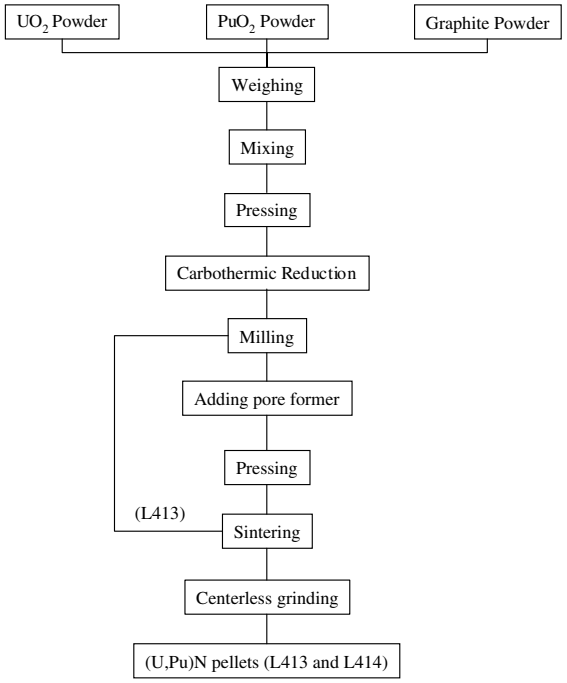

Fig. 1. Flow sheet for fabrication of (U,Pu)N pellets.

Table 2
Chemical analyses of fuel pellets

Fuel pin number	L413	L414
N (wt%)	5.56	5.62
C (wt%)	0.11	0.16
O (wt%)	0.02	0.02
Impurity elements (wt ppm)		
Al	70	30
B	<10	<10
Ca	40	40
Cd	<10	<10
Co	170	90
Cr	60	30
Fe	50	30
Mg	30	20
Ni	30	30
V	230	50
W	1280	530
Cu + Si + Zn	200	140
Ag + Mn + Mo + Pb + Sn	80	90

0.45 mm, respectively. The length of the fuel column was approximately 200 mm. Fig. 2 shows a schematic illustration of the nitride fuel pin and its configuration in the fuel assembly during irradiation. These fuel pins were loaded into a PFB090 fuel assembly, which was an uninstrumented irradiation subassembly type B (UNIS-B) of JOYO. The UNIS-B is a compartment type subassembly, which can be reloaded in the reactor core after interim examination of test fuel pins. Two (U,Pu)N fuel pins were installed in the compartment L4C4. A schematic diagram of the L4C4 compartment and PFB090 fuel assembly are shown also in Fig. 2. These fuel pins were spaced not by the wrapping wire, but by the grid type supports.

2.2. Irradiation conditions

The PFB090 fuel assembly was placed in the third row positioned next to the control rod in the JOYO MK-II core. Irradiation of the PFB090 fuel assembly spanned five reactor cycles (from the 29th to the 33rd cycles) equivalent to 276 effective full power days. The maximum linear heating rate was about 75 kW/m, which was recorded in the first stage of the irradiation period, and peak burn-up reached around 4.3% FIMA. The power history and burn-up evolution are shown in Fig. 3. After the irradiation, fuel pins were withdrawn from the fuel assembly for the post irradiation examinations.

3. Experimental procedure

3.1. Nondestructive examinations and puncturing

Diameter measurements were carried out on the irradiated fuel pins by a conventional method. The cladding diameter was continuously measured along the axis of the fuel pin at intervals of 1 mm and 15° in the circumferential angle. The amount of fission gas released from fuel pellets to the free space in the fuel pins was measured by the pin-puncturing test.

3.2. Optical microscopy and quantitative image analysis

The irradiated fuel pins were cut at different axial positions into several segments and the cross section was ground and polished using water-free lubricant in order to avoid a reaction between water and (U,Pu)N fuel. The microstructure on the cross section was observed with a optical microscope (FAROM of Union Optical) and digitally recorded. In order to investigate the distribution of pores, quantitative image analysis was carried out on optical micrographs using the software Win ROOF ver.3.5 (Mitani Corp.).

3.3. Scanning electron microscopy (SEM)

SEM was performed with the JSM50A model (JEOL). The electron column and specimen chamber were shielded with lead and tungsten blocks for radiation protection. The secondary electron detector was also shielded with tungsten against gamma rays from

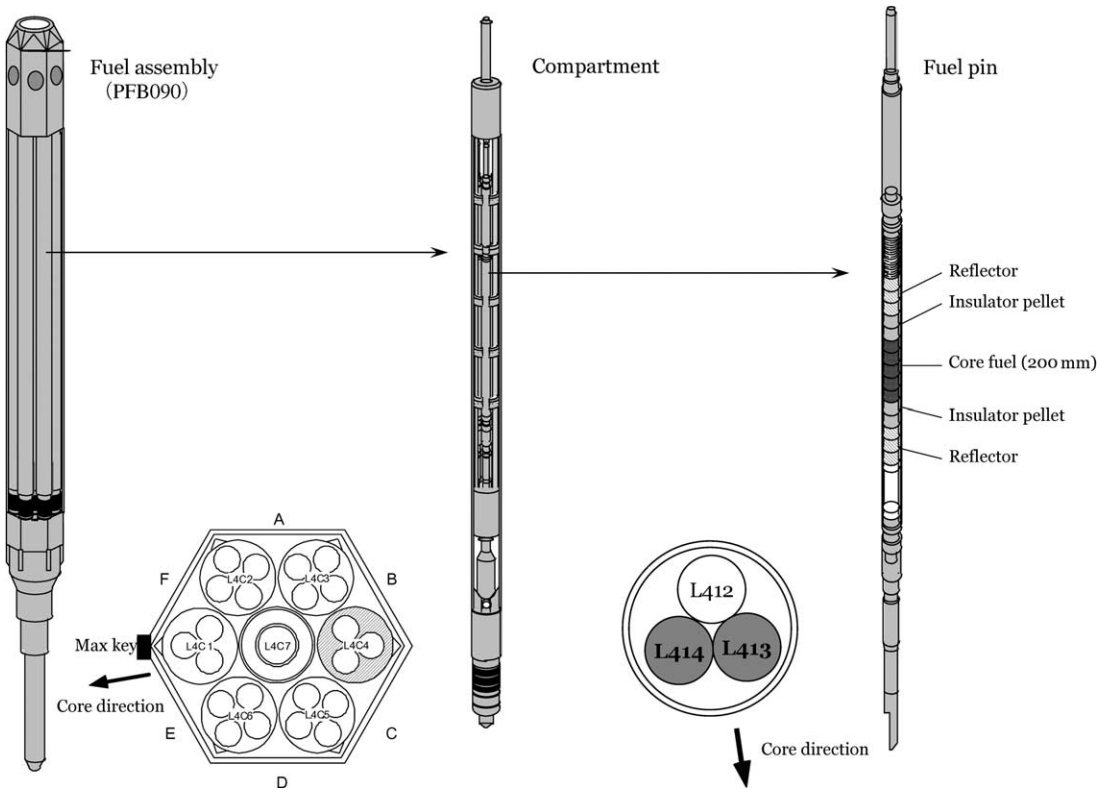

Fig. 2. Structure of fuel pins for irradiation test in JOYO.

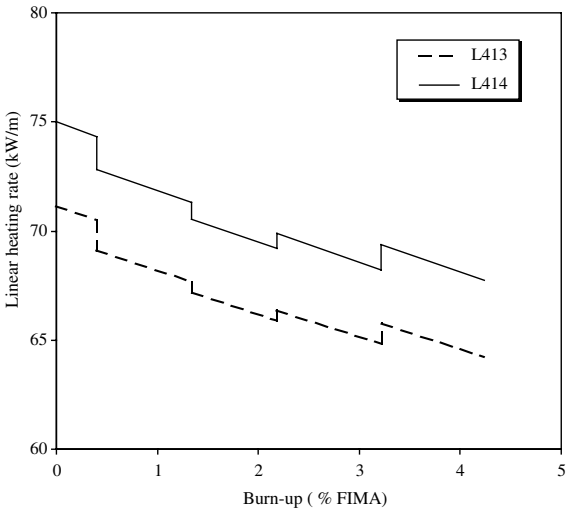

Fig. 3. Irradiation conditions of (U,Pu)N fuel pins.

irradiated specimens. The specimen surface was polished and coated with a thin layer of carbon by vacuum evaporation to avoid electron charging effects.

3.4. Electron probe microanalysis (EPMA)

EPMA was performed with the CAMEBAX-R model (Cameca) which was specially shielded with lead and tungsten to permit the analysis of irradiated nuclear fuels. Xe radial distributions were measured at an electron acceleration potential of 25 kV and incident beam current of 1 μA, and the acquisition time was 20 s. Under these conditions, the depth of electron beam penetration from the surface of specimen is about 0.5 μm. The incident beam diameter during the measurement was controlled at 50μm in order to acquire the average value of excited X-rays from a wide region.

Xe was analyzed using the $L\alpha$ line of the characteristic X-ray and LiF diffracting crystal. Quantitative analysis of Xe was carried out using the calibration curve from the data of standard specimens. In this study, the outermost part of the MOX fuel irradiated to low burn-ups at low temperature in the JOYO MK-II core was applied as the standard specimen, assuming that all the Xe produced in the fuel region was retained. This method was similar to one described elsewhere [6]. The specimen surface was polished using standard metallographic techniques. A thin film of carbon was applied to

the specimen surface by vacuum evaporation to ensure good electrical conductivity.

3.5. Density and open porosity measurements

After the segment cutting, an attempt was made to separate the fuel pellet from the cladding tube; this was unsuccessful because bonding material laid between the fuel and cladding. Then, the pellet was removed by longitudinally splitting the cladding tube. One whole pellet was removed from the L414 fuel pin, while seven pieces representative of a whole pellet were collected from the L413 fuel pin.

Before irradiation, density of the fuel pellets was measured using the geometrical volume and weight of a pellet. But after irradiation, it was measured by two methods; one was the pycnometric method using mercury and the other was the immersion technique using *m*-xylene, because a number of cracks occurred in the fuel pellets due to thermal stress, and in some cases the pellet was divided into several pieces.

Since mercury does not enter the open pores but *m*-xylene does, the fraction of open pores could be determined from the values measured by the two methods.

3.6. Fuel specimens for destructive examinations

In the L413 fuel pin, the microstructure was observed on one cross section at the axially middle position $X/L = 0.49$, where X is the distance from the bottom of the fuel column and L is the total length of the fuel column. On the other hand, in the L414 fuel pin, microstructures were observed on three cross sections, upper ($X/L = 0.95$), middle (0.5) and lower (0.06) positions. Specimens for the density measurement were also taken from the regions of $X/L = 0.65$–0.75 in L413 and of $X/L = 0.65$–0.80 in L414.

4. Results

4.1. Profilometry of cladding

The diameters of irradiated fuel pins were measured as a function of the distance from the bottom of the fuel pin. Twelve diameter measurements were carried out at every circumferential interval of 15°.

Fig. 4 shows the average values of the 12 diameter measurements and the diameters measured at A–C and B–D directions, which made a right angle to each other. The axial profiles of the diameters measured as the

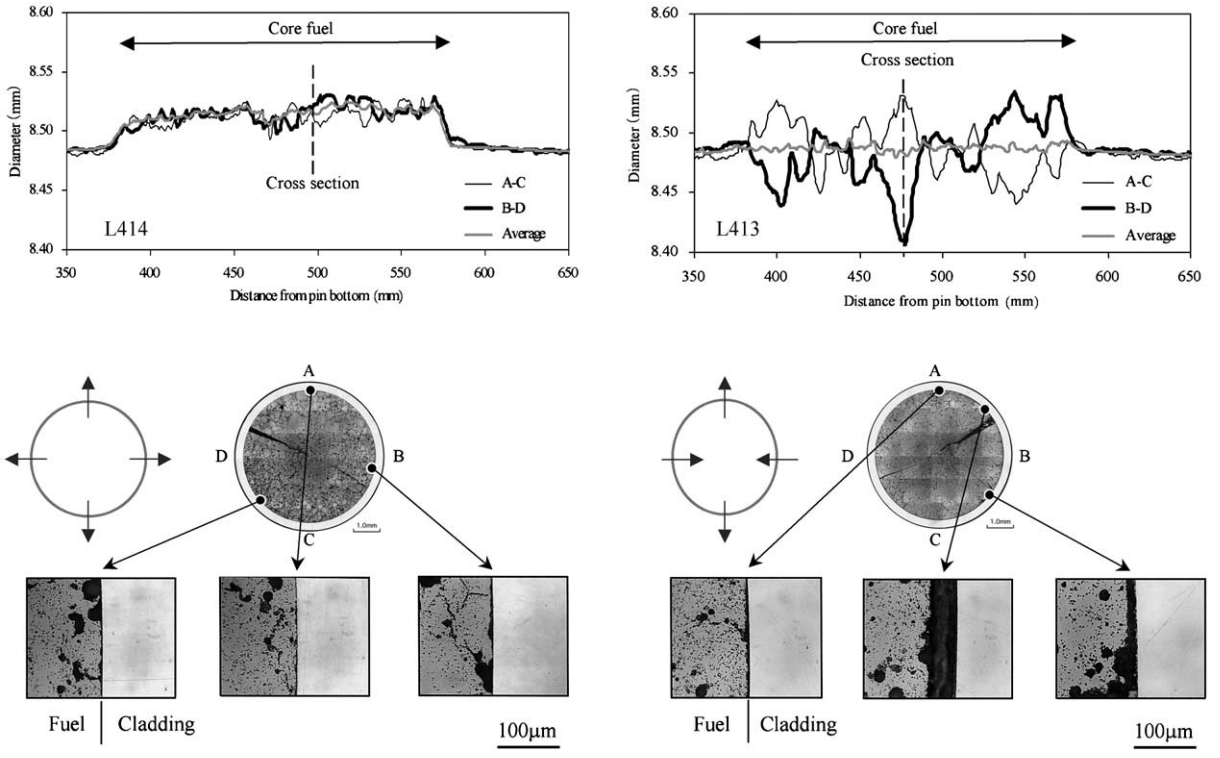

Fig. 4. Profilometry results and cross-sectional structure of fuel pins.

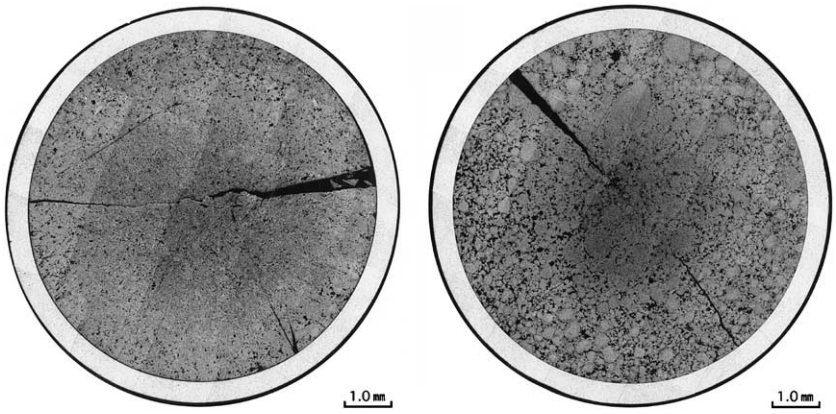

Fig. 5. Microstructures of middle position of irradiated (U,Pu)N fuel pins.

average of 12 measurements and at A–C and B–D directions were nearly the same for L414. The maximum value of $\Delta D/D$ was about 0.51%, where D is the diameter of the fuel pin before the irradiation, and ΔD is the increase of diameter due to irradiation.

On the other hand, little increase was seen in the average diameter of the L413 fuel pin before and after the irradiation, but a distinct change was found in the diameter at the two circumferential angles, which made a right angle to each other, showing prominent ovalities. The maximum value of $\Delta D/D$ of the L413 fuel pin was about 0.17%.

Two tendencies could be explained from the enlarged microstructure of the cross sections shown in Fig. 4. On the cross section of the L414 fuel pin for which diameters increased at all radial angles, the fuel-cladding gap closed. On the cross section of the L413 fuel pin, however, the gap was open in the radial direction where the diameter decreased, while it was closed in the direction where the diameter increased.

4.2. Microstructures

Fig. 5 shows the microstructures of irradiated fuel pins on the cross section at the middle position. No remarkable evolutions of central void and columnar grains could be seen in the microstructures, although the fuel pins were irradiated at high liner heating rate (>70 kW/m) in comparison with the MOX fuels. Radial cracks were observed, which were probably introduced by thermal stresses during the initial startup. The pores, which were introduced during the fabrication process, were also observed throughout the pellet cross section. The 'island-like structure' pointed out by Prunier et al. [7], which looks like a highly dense island surrounded by a porous matrix, was observed throughout the cross sections for specimens taken at three different axial positions of the L414 fuel pin.

4.3. Density and porosity

Table 3 lists the results of density and porosity measurements. The density of fuel pellets measured by the pycnometric method decreased by about 5.8% and 5.4% in the L413 and L414 fuel pins, respectively, compared with densities before irradiation. These values corresponded to volume swelling of about 7.4% and 6.7%, from which the swelling rates were calculated to be 1.8%/% FIMA and 1.6%/% FIMA. From the comparison between the values measured by the pycnometric method and the immersion technique, the fractions of open and closed porosity were obtained. As shown in Table 3, the fractions of open pores in both fuel pellets were about 4%.

Fig. 6 shows the areal fraction of pores, which was obtained from the image analysis on the cross section of $X/L = 0.5$ for the L414 fuel pin. The areal fraction of pores increased in the direction of the fuel pellet center.

Table 3
Density and porosity measurements and fission gas release rate

	L413	L414
Density (before irradiation) (%T.D.)	84.8	86.0
Density (after irradiation) (%T.D.)	79.0	80.6
Swelling (%)	7.4	6.7
Swelling rate (%/%FIMA)	1.8	1.6
Open porosity (%)	4.2	4.1
Closed porosity (%)	16.8	15.3
Fission gas release rate (%)	3.3	5.2

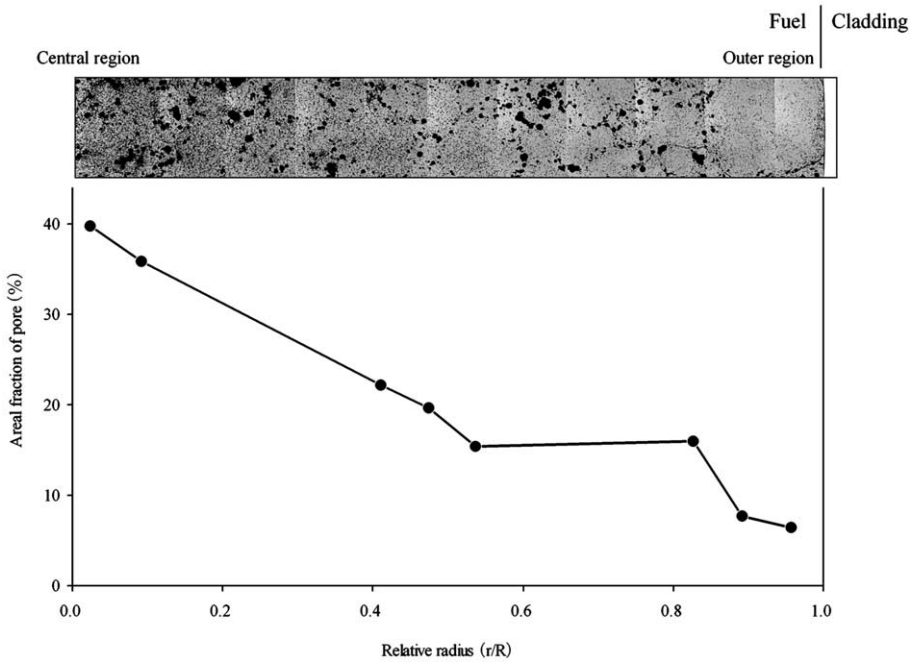

Fig. 6. Radial distribution of the areal fraction of pores as obtained by image analysis.

This tendency could be attributed to the formation of fission gas bubbles, that is, fission gas bubbles grew more easily in the central region than in the outer region.

Fig. 7 shows the secondary electron micrograph around the central region of the L414 fuel pellet. A number of fission gas bubbles were formed and some of them connect with each other. However, tunnel formation resulting in fission gas release as seen in irradiated oxide fuel was not present.

4.4. Fission gas release rate

Table 3 also shows the fission gas release rate in both fuel pins measured by pin-puncturing test. The release rates of L413 and L414 fuel pins were about 3.3% and 5.2%, respectively. These values were smaller than those of MOX fuel pins irradiated to the same level of burn-up [8].

Fig. 8 shows the burn-up dependence of the fission gas release rate obtained in the present study with the data of previous studies by Storms [9], Iwai et al. [10] and Blank et al. [11]. The burn-up dependence of fission gas release rates obtained in the present study was similar to the literature data.

4.5. Radial distribution of xenon

The radial distribution of Xe on the cross section at the middle position $(X/L = 0.5)$ of the L414 fuel pin is shown in Fig. 9. The dotted flat line shows the generated Xe concentration theoretically calculated by ORIGEN2 code. The Xe concentration measured by EPMA decreased in the direction of the fuel pellet center.

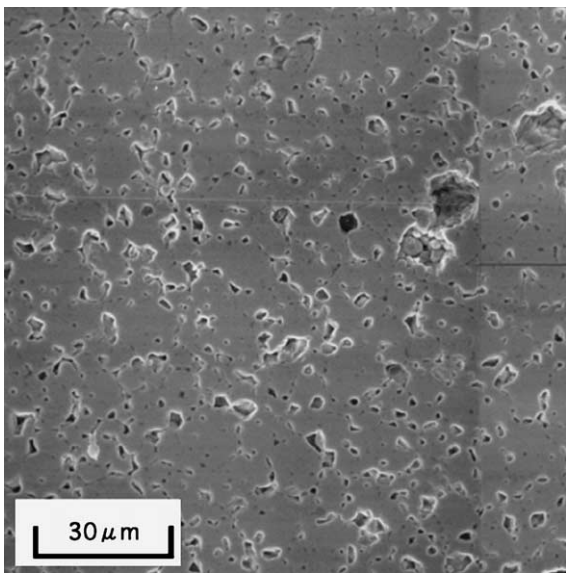

Fig. 7. Secondary electron image in the central region of irradiated fuel (L414).

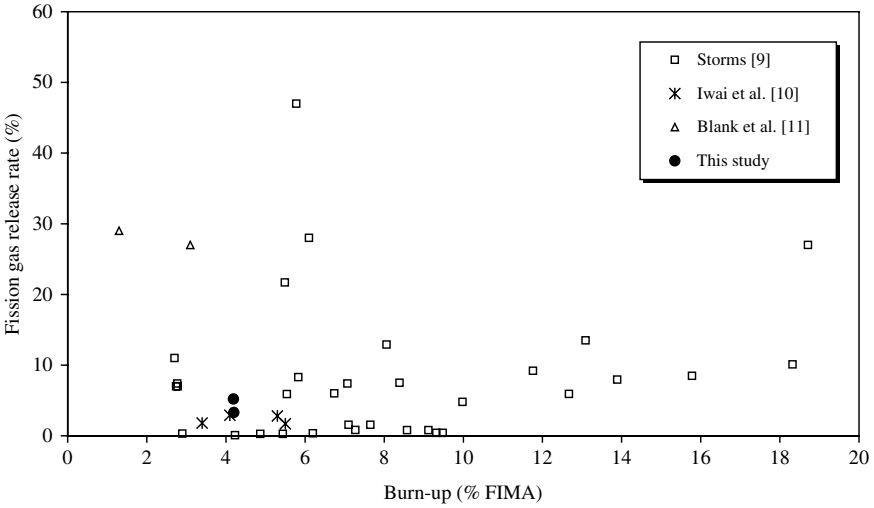

Fig. 8. Fission gas release rate of nitride fuels.

5. Discussion

5.1. Fission gas release

Bauer et al. [12] analyzed the fission gas release data as a function of porosity in the mixed nitride fuel. They pointed out that at densities greater than about 85% TD, gas release can be basically accounted for by recoil from the geometric surface of the pellet, and at lower densities, gas release increases rapidly with decreasing density indicating that gas is being released through surface-connected porosity. Fig. 10 compares the present data and their data. The present data were in good agreement with the previous data.

From the measurement of open porosity and microscopic observations on the central region of the fuel pellet, it was considered that the precipitated fission gas bubbles were retained on the grain boundary in this central region. Therefore, fission gas release in the (U,Pu)N fuel pins irradiated in JOYO was mainly caused by recoil on the surface of the pellet, open pores and cracks, which were exposed to the free space in the fuel pin.

5.2. Evaluation of fission gas retained in the fuel

As shown in Figs. 6 and 9, the Xe concentration decreased and the porosity increased in the central region. In the direction of fuel pellet center, the mobility of fission gas atom increased with rising temperature, and subsequently the formation and coalescence of fission gas bubbles occurred easily.

When the Xe concentration retained in the fuel pellet is measured by EPMA, the detected intensity of the characteristic X-rays changes, depending on the condition of the fuel region including Xe atoms. That is, the detection efficiency of Xe in the fission gas bubble is significantly different from that in the matrix. When the detectable intensity in the fission gas bubble with a diameter larger than 0.05 μm is compared with the detectable intensity in the fuel matrix, the former intensity decreases to about 70% of the latter [13]. It was previously reported that the diameter of fission gas bubbles precipitated in the intragranular region is less than 0.04 μm [14] and fission gas concentration can be detected by EPMA. However, when the diameter of the fission gas bubbles formed on the grain boundary is larger than 0.1 μm, its concentration cannot be detected by EPMA. Therefore, the increase of pore size leads to the decrease of detection efficiency of Xe in the fuel region.

In the L414 fuel pin, the Xe concentration retained in the intragranular region of fuel was evaluated from the EPMA results. When the radial Xe concentration profiles are measured by EPMA for the cross sections at n-axial positions, the general method to derive the total amount of Xe in the intragranular region from the EPMA results is shown in Fig. 11 and given by the following equations:

$$A_j = \sum_i \cdot\pi \cdot (r_{i+1}^2 - r_i^2) \cdot \frac{(M_{i+1} + M_i)}{2}, \tag{1}$$

$$W = \sum_{\substack{j\neq 1 \\ j\neq n}} \frac{1}{2} + (l_{j+1} - l_{j-1}) \cdot A_j + \frac{1}{2}(l_2 + l_1) \cdot A_1 + \left\{ l - \frac{1}{2}(l_n + l_{n-1}) \right\} \cdot A_n, \tag{2}$$

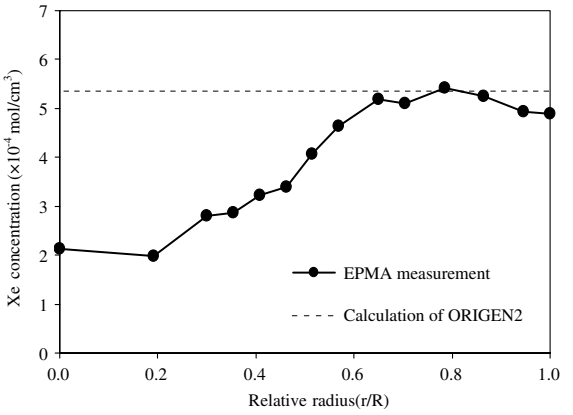

Fig. 9. Radial distribution of Xe in the middle position of L414 fuel pin.

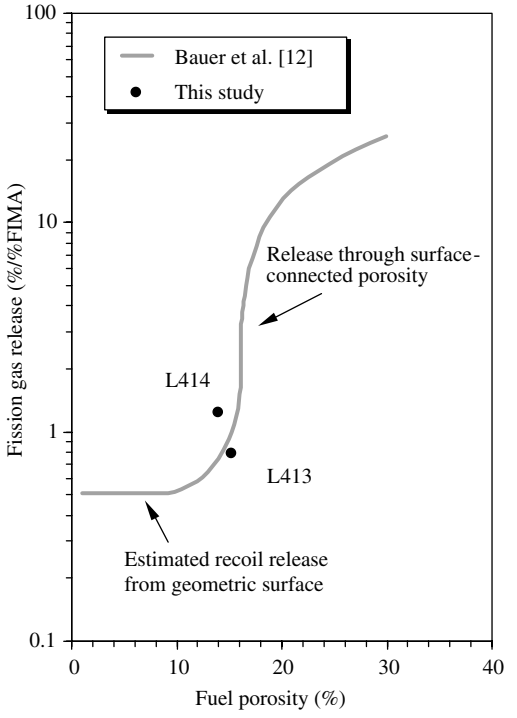

Fig. 10. Fission gas release dependence on (U,Pu)N pellet density.

A_j retained concentration on the cross section of the pellet in the position j (mol/cm)
r_i distance from the center of the pellet to the radial position i (cm)
M_i Xe concentration at the radial position i (mol/cm^3)
W the amount of retained Xe of a fuel pin (mol/pin)
l_j distance from core bottom to the axial position j (cm)
l fuel column length (cm)

In the L414 fuel pin, the radial Xe concentration profiles were measured on three cross sections at axial positions of $X/L = 0.95$, 0.5 and 0.06 by EPMA. If this method is applied to the analysis in this study, the axial length of the fuel is divided into three sections by two mean values between the axial positions on which cross sections the radial Xe concentration profiles were measured. In each section, the radial Xe concentration profile was represented by the one measured in this section. The total amount of fission gas in the intragranular region was calculated using the Eqs. (1) and (2), and the result was 3.18×10^{-3} mol/pin. In addition, the total amount of fission gas generated in the whole fuel region was calculated by ORIGEN2 and the result was 3.95×10^{-3} mol/pin. From the comparison between both values, the fraction of fission gas retained in the intragranular region is about 80%. On the other hand, about 5% of the fission gas release was measured by the pin-puncturing test. Thus, the fraction of fission gas retained in the fission gas bubbles is estimated as about 15%. The fraction of Xe retained in the intragranular region is higher than that of MOX fuel pins irradiated to the same degree of burn-up [6].

Coquerelle and Walker [15] investigated the fission gas release for (U,Pu)N irradiated at the liner heating rate of 115 kW/m to 1.1% FIMA in DFR. They reported that the Xe release was approximately 45% in the region from $r/R = 0$ to 0.85 and 15% in the outer part of the fuel. The linear heating rate was higher in their study than in the present case. It is, therefore, suggested that the fission gas release took place by the diffusion process in their study.

5.3. Fuel swelling

Fission gas release is generally smaller in nitride fuel than in oxide fuel, because the better thermal conductivity of nitride fuel results in a low temperature. The large fraction of fission gas retained in the fuel, however, may lead to a large swelling rate when fuel temperature becomes high enough to form bubbles.

Lyon et al. [16] and Blank and Bokelund [17] separately reviewed past experimental data on irradiated nitride fuel, and both recommended that the swelling rate is 1.5%/% FIMA. In addition, Bauer et al. [18] reported that the swelling rate is 1.83%/% FIMA without the constraint of cladding and is 1.44%/% FIMA under constraint of cladding for the nitride fuel irradiated to 9.3% FIMA. In this study, swelling rates of 1.8 and 1.6%/% FIMA are obtained in the L413 and L414 fuel pins, respectively. Both

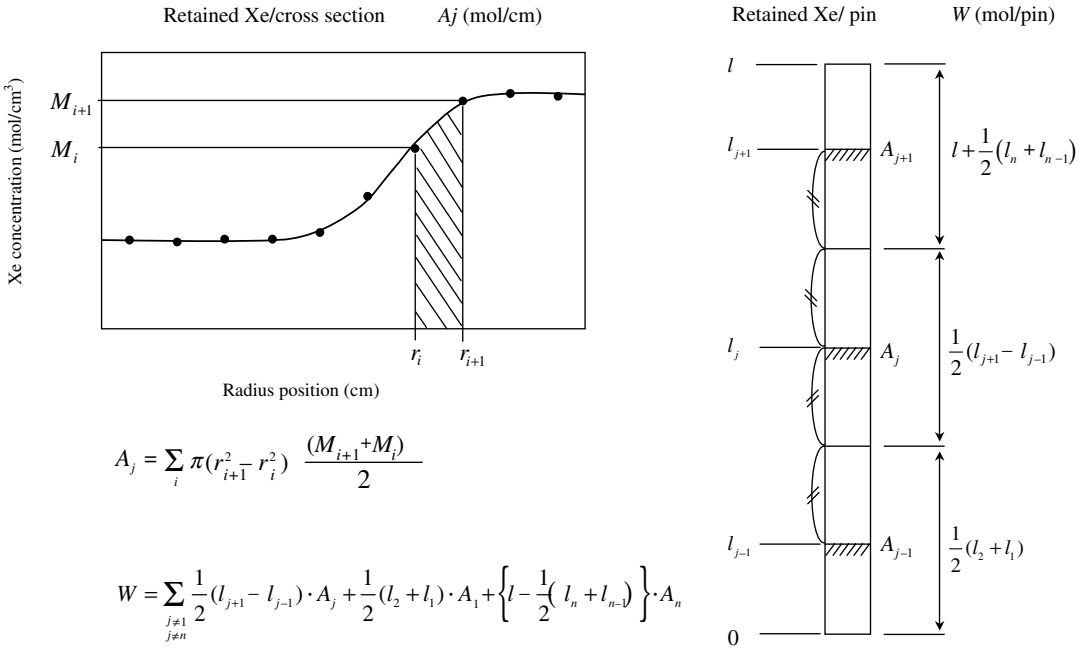

Fig. 11. Schematic diagram of calculation method of retained Xe.

values show a reasonable agreement with the above data.

Fuel swelling has a significant effect on FCMI. The cladding diameter increases uniformly in the L414 fuel pin with a smaller fuel-cladding gap. In the L413 fuel pin with a larger fuel-cladding gap, however, it increases at one circumferential angle, but decreases at the right angle to that one. Ovality of advanced LMFBR fuel pins has been observed previously [19]. In the present study, since there is no spacer wrapping wire for either fuel pins, external forces cannot cause the ovality.

The difference in diametral changes between the L413 and L414 fuel pins can be explained by relocation of the fuel fragments. In the L414 fuel pin with a smaller gap width, the free space in the cladding is too narrow for the fuel fragments to move freely. This limits the relocation of the fuel fragments so that the cladding deforms uniformly with the increase of fuel swelling during irradiation. On the other hand, in the L413 fuel pin with a larger gap width, the space inside the fuel pin is so wide that the fuel fragments move freely. These fragments can be relocated to contact the cladding or wedge against it. Either difference in thermal expansions between the fuel and cladding or fuel swelling during steady-state operation can lead to the localized fuel cladding mechanical interactions that cause ovalities. From this finding, it is concluded that the larger fuel-cladding gap aiming at the accumulation of fuel swelling is not reasonable for He-bonded nitride fuel pins.

6. Conclusion

Two uranium–plutonium mixed nitride, (U,Pu)N, fuel pins with different He-gap width were irradiated at a linear heating rate 75 kW/m to 4.3% FIMA in the experimental fast reactor JOYO. Subsequently, nondestructive and destructive post irradiation examinations were carried out in hot cells. In particular, fission gas and swelling behavior during irradiation were investigated in detail. The results are summarized as follows.

- Fission gas release rates in the two fuel pins were about 3.3% and 5.2%, and their swelling rates were about 1.8 and 1.6%/% FIMA.
- From the radial distributions of Xe concentration measured by EPMA, it was determined that about 80% and 15% of the fission gases were retained in the intragranular region and in the fission gas bubbles, respectively.
- Uniform deformation of the cladding due to FCMI was observed in the fuel pin with a smaller gap width, but significant ovalities were seen in the fuel pin with a larger gap width. In the latter, the large space for the movement of the fuel fragments led to the nonuniform relocation, resulting in the oval deformation of the cladding.
- It was concluded that the larger fuel-cladding gap aiming at accumulating the fuel swelling would not be reasonable for He-bonded nitride fuel pins.

To demonstrate the irradiation performance of nitride fuel for fast reactors, it is necessary to carry out irradiation tests aiming at higher burn-up hereafter. From the viewpoint of mitigating FCMI, the proper fuel design and porosity control manner of nitride fuel may also be required.

Acknowledgements

The authors are grateful to Dr H. Furuya (Emeritus professor of Kyushu university), and Dr M. Ito and Mr T. Asaga (Japan Nuclear Cycle Development Institute) for their suggestions and discussions in this study. They also thank to Messrs Y. Ohsato, Y. Onuma, S. Nukaga, Y. Haga (Nuclear Technology and Engineering Corporation) for help in the experiments.

References

[1] Hj. Matzke, Science of Advanced LMFBR Fuels, North-Holland, Amsterdam, 1986.
[2] H. Blank, in: Materials Science and Technology, in: B.R.T. Frost (Ed.), Nuclear Materials, vol. 10A, VCH, Weinheim, 1994.
[3] H. Blank, J. Less-Common. Met. 121 (1986) 583.
[4] H. Blank, M. Coquerelle, I.L.F. Ray, K. Richter, C.T. Walker, in: Proceedings on Reliable Fuels for Liquid Metal Reactors, Tucson, AZ. 7–11 September 1986, p. 7-15.
[5] Y. Arai, S. Fukushima, K. Shiozawa, M. Handa, J. Nucl. Mater. 168 (1989) 280.
[6] S. Ukai, T. Hosokawa, I. Shibahara, Y. Enokido, J. Nucl. Mater. 151 (1988) 209.
[7] C. Prunier, P. Bardelle, J.P. Pages, K. Richter, R.W. Stratton, G. Ledergerber, in: Conference on Fast Reactors and Related Fuel Cycles (FR'91), Kyoto, 28 October–1 November 1991, p. 15.9-1.
[8] H. Kashihara, S. Shikakura, Y. Yokouchi, I. Shibahara, H. Matsushima, K. Yamamoto, Fast reactor core and fuel structural behaviour, in: Proceedings of International Conference Organized by BNES, Inverness, 4–6 June 1990, BNES, London, p. 243.
[9] E.K. Storms, J. Nucl. Mater. 158 (1988) 119.
[10] T. Iwai, K. Nakajima, Y. Arai, Y. Suzuki, IAEA Tech. Committee Meeting on Research of Fuel Aimed at Low Fission Gas Release, Moscow, 1–4, 1996, p. 137.
[11] H. Blank, K. Richter, M. Coquerelle, Hj. Matzke, M. Campana, C. Sari, I.L.F. Ray, J. Nucl. Mater. 166 (1989) 95.
[12] A.A. Bauer, J.B. Brown, E.O. Fromm, V.W. Storhok, in: Proceedings on Fast Reactor Fuel Element Technology, 1971, p. 785.
[13] C. Ronchi, C.T. Walker, J. Phys. D: Appl. Phys. 13 (1980) 2175.
[14] C. Ronchi, Hj. Matzke, Fuel and Fuel Elements for Fast Reactors, IAEA, Vienna, 1974, p. 57.
[15] M. Coquerelle, C.T. Walker, Nucl. Technol. 48 (1980) 43.
[16] W.F. Lyon, R.B. Baker, R.D. Leggett, R.B. Matthews, in: Conference on Fast Reactors and Related Fuel Cycles (FR'91), Kyoto, 28 October–1 November 1991, p. 14.8-1.
[17] H. Blank, H. Bokelund, IAEA-TECDOC-352, 1985, p. 189.
[18] A.A. Bauer, P. Cybulskis, R.L. Petty, N.S. Demuth, in: Proceedings of International Conference on FBR Fuel Performance, Monterey, CA, 3–5 March 1979, p. 827.
[19] J.F. Kerrisk, J.O. Barner, R.L. Petty, Nucl. Technol. 30 (1976) 361.